

Stability analysis and energy harvesting in lumped parameter systems with internally coupled resonators

Alimohammadi, Hossein; Vassiljeva, Kristina; HosseinNia, S. Hassan; Petlenkov, Eduard

DOI

[10.1177/10775463241241161](https://doi.org/10.1177/10775463241241161)

Publication date

2024

Document Version

Final published version

Published in

JVC/Journal of Vibration and Control

Citation (APA)

Alimohammadi, H., Vassiljeva, K., HosseinNia, S. H., & Petlenkov, E. (2024). Stability analysis and energy harvesting in lumped parameter systems with internally coupled resonators. *JVC/Journal of Vibration and Control*, 31 (2025)(7-8), 1210-1222. <https://doi.org/10.1177/10775463241241161>

Important note

To cite this publication, please use the final published version (if applicable). Please check the document version above.

Copyright

Other than for strictly personal use, it is not permitted to download, forward or distribute the text or part of it, without the consent of the author(s) and/or copyright holder(s), unless the work is under an open content license such as Creative Commons.

Takedown policy

Please contact us and provide details if you believe this document breaches copyrights. We will remove access to the work immediately and investigate your claim.

Stability analysis and energy harvesting in lumped parameter systems with internally coupled resonators

Hossein Alimohammadi¹ , Kristina Vassiljeva¹ , S Hassan HosseinNia² , and Eduard Petlenkov¹ 

Journal of Vibration and Control
2024, Vol. 0(0) 1–13
© The Author(s) 2024



Article reuse guidelines:

sagepub.com/journals-permissions

DOI: 10.1177/10775463241241161

journals.sagepub.com/home/jvc



Abstract

This article explores internally coupled resonators in metamaterial systems, focusing on mechanical and electromechanical coupling. The article provides a thorough examination of stability within the context of internally coupled resonators. It establishes stability criteria, emphasizing the importance of strictly stable systems in practical applications. Furthermore, it analyzes stability through simulations, revealing how various parameters impact system behavior and highlighting the challenges and benefits of achieving stability in metamaterial systems. Additionally, the article explores the impact of damping coefficients and resonator characteristics, on displacement and power generation profiles. Nonlinear behavior in internally coupled resonators is examined, revealing the presence of bifurcation in simulation and offering insights into multi-stability and system behavior.

Keywords

stability, internally coupled resonators, piezoelectric energy harvesting, vibration suppression, lumped systems

1. Introduction

Internally coupled resonators, integral in wave control, stability, and energy collection, are crucial in lumped parameter systems' engineering. This article emphasizes the role of these resonators, highlighting the benefits of mechanical linear, nonlinear internal coupling, and electro-mechanical shunt capacitance circuits. These mechanisms allow for negative stiffness and refined system dynamic control. Electrical internal coupling, as shown through simulations, offers tunability and superior energy harvesting. Moreover, the article examines how parameters like damping coefficients and resonator traits influence displacement and energy output at varied frequencies. The nonlinear aspects of these resonators, leading to multi-stability and specific system behaviors, are also explored.

and directing wave propagation, establishing themselves as invaluable resources in various fields, such as structural health monitoring, acoustic metamaterials, and vibration mitigation. Notable research in this field, particularly exemplified by the studies of Hu et al. (2018), has traversed through metastructures featuring linearly coupled resonators. The discoveries from such investigations illuminate the existence of an additional narrow band gap in comparison to conventional metastructures, thereby highlighting the fascinating potentialities within this area of research.

While the concept of employing negative stiffness has been explored extensively in past research, Liu et al. (2022) delve into a diatomic-chain locally resonant acoustic metamaterial structure, underscoring the pivotal role of the

1.1. Internally coupled resonators exhibiting mechanical nonlinearity

The emergence of internally coupled resonators has been identified as a key element in recent dynamics and vibration control research. Through the complex interactions among internal structural components, these resonators exhibit a varied array of vibrational behaviors. These distinctive properties afford unprecedented capabilities in managing

¹Department of Computer Systems, Tallinn University of Technology, Tallinn, Estonia

²Department of Precision and Microsystems Engineering, Delft University of Technology, Delft, The Netherlands

Received: 25 October 2023; revised: 13 January 2024; accepted: 27 February 2024

Corresponding author:

E Petlenkov, Department of Computer Systems, Tallinn University of Technology, Akadeemia tee 15a, Tallinn 12618, Estonia.

Email: eduard.petlenkov@taltech.ee

negative-stiffness mechanism in enhancing vibration suppression. By utilizing additional band gaps and Bragg scattering, the structure exhibits superior management of vibration transmission, particularly in managing ultralow frequency vibrations in the lower frequency spectrum. The negative-stiffness mechanism proves vital for fine-tuning the metamaterial's band gap characteristics and potential applications in vibration reduction, especially under specific material parameters.

1.2. Electromechanical internally coupled resonators

Electromechanical resonators, notably those incorporating piezoelectric elements and internal coupling of resonators, manifest a compelling complexity by merging mechanical and electrical aspects, thus enabling unique wave propagation properties. While their promising attributes are evident, an exploration into nonlinear, internally coupled electromechanical systems is relatively untapped. This discernible gap in research accentuates the need for an exhaustive study of these systems, which have the capacity to innovate vibration control and energy-harvesting sectors (Shu and Lien, 2006; Lefeuvre et al., 2005).

Despite their remarkable wave propagation features, metamaterials are often hindered by the limited bandwidth of their band gaps, impacting their performance in broad-spectrum vibration applications. To counteract this, research has pivoted toward developing metamaterial configurations with multiple band gaps and utilizing nonlinearity as a powerful tactic (Fang et al., 2017). The characteristics of piezoelectric shunt methods, marked by their mechanical–electrical conversion capabilities, have spurred research into dynamically tunable metamaterials. However, most studies predominantly utilize independent piezoelectric shunt circuits for each local resonator (Chatziathanasiou et al., 2022; Li et al., 2023).

The primary objective of this study is to comprehensively examine the band gap characteristics of the proposed lumped system, emphasizing the mechanical and electromechanical internal coupling through the shunt capacitance circuit and conceptualizing the circuit as a negative capacitor (Hu et al., 2017). Additional goals involve conducting a stability analysis of the piezoelectric elements model on the resonator and a pivotal comparison of power and energy harvested from the resonators, with a special focus on their impact on band gap formation in the chain mass structure.

1.3. Solution stability

The stability and singularity of nonlinear solutions in mechanical internally coupled resonators,

electromechanical internal coupling, and other nonlinear periodic media have been somewhat overlooked. Stability analysis regarding wave responses in phononic media is documented in foundational systems (Newton and Keller, 1987), works addressing geometric nonlinearity (Liu et al., 2022; Murer et al., 2023), and studies on topological modes (Chaunsali et al., 2021). The introduction of nonlinearity often induces bifurcations, leading to dynamic solutions with multiple branches. Without a stability analysis, theoretical responses might not represent physical systems accurately. Investigations into the stability of harmonic excitations have revealed transitions between stable solutions with increasing amplitude, eventually leading to chaotic dynamics (Hoogeboom et al., 2013).

Meanwhile, stability analysis of plane waves in nonlinear phononics remains relatively unexplored. Newton and Keller (Newton and Keller, 1987) introduced an equation to assess the perturbation growth rate to ascertain the start and end of plane wave stability. Further studies by Fronk and Leamy (Fronk and Leamy, 2017, 2019) addressed plane wave stability in monoatomic and diatomic chains. These findings highlight that in 1D systems, stability is amplitude-dependent, and in 2D, it also depends on direction. Recent studies have also analyzed the stability of topologically protected modes (Mančić et al., 2023) in highly nonlinear systems, unveiling specific frequency–energy domains where the protected mode becomes unstable.

This research tackles the challenge of optimizing band gap characteristics and energy harvesting in linear and nonlinear internally coupled resonators, a significant gap in current metamaterial applications crucial for advancing energy efficiency and vibration control.

The primary contributions of this paper are summarized as follows:

- Analyzed band gap and energy harvesting in nonlinear coupled resonators in lumped system.
- Developed new stability analysis for nonlinear resonator systems.
- Identified enhancements in band gaps specifically in internally coupled resonators.
- Illustrated how internal coupling boosts energy harvesting and analyzed damping impacts.
- Provided insights on optimizing metamaterials for energy harvesting.
- Demonstrated advantages of electromechanical shunt circuits in tuning band gaps.

2. Method

Using the lumped parameter model, intricate physical systems are distilled into discrete points defined by parameters such as resistance, capacitance, or mass. This is

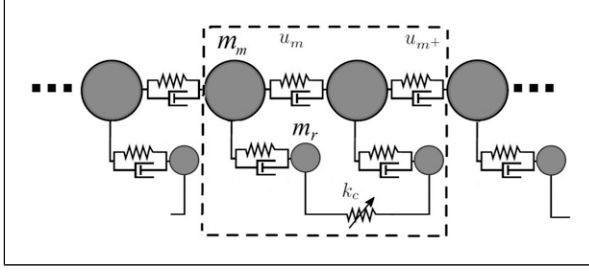


Figure 1. A mechanically internally coupled resonator. The dashed rectangle signifies a unit cell.

suitable for systems where the wave propagation wavelength far exceeds structural dimensions.

Through the Lagrangian energy method, equations of motion are derived for metamaterials interfaced with internally coupled resonators. Given the system's inclusion of negative stiffness, an essential stability analysis is executed, aiming for vibration suppression enhancements while ensuring stability and reliability.

2.1. Linear electromechanical resonators

In electromechanical systems employing piezoelectric elements, additional nonlinearity is introduced to the system dynamics, serving to dampen vibrations and enhance energy harvesting in resonators. When resonators are integrated with piezoelectric elements, a coupling between mechanical and electrical dynamics occurs, which enriches yet complicates system behavior. Utilizing Lagrange's equation, governing dynamics can be obtained, with mechanical damping typically represented via Rayleigh damping and energy equations being linearly characterized. The resulting governing equations of motion are delineated accordingly.

2.2. Analysis of power output of standard piezoelectric circuit for energy harvesting

In investigating the nonlinearity properties in piezoelectric materials, this study utilizes a standard circuit paired with each nonlinearity type. This approach ensures that each nonlinearity is observed in isolation, unaffected by different circuit efficiencies. Here, the piezo voltage, $v_p(t)$, has a direct proportionality to the displacement, $u(t)$. An in-depth analysis yields the average harvested power P in the system as

$$P = \frac{v_c^2}{R} = \frac{R\theta^2\omega^2}{\left(Rc_p\omega + \frac{\pi}{2}\right)^2 z_0^2} \quad (1)$$

This formulation encapsulates the intricate interplay between electric charge storage, current dynamics,

mechanical displacement, and the system's power harvesting (Shu and Lien, 2006).

2.3. Internally coupled resonators with mechanical nonlinearity

The system, illustrated in Figure 1, embodies a nonlinear mechanical chain internally coupled, with a unit cell delineated by a dashed rectangle. The analysis simplifies the system dynamics by exclusively considering springs, assuming linearity for both the primary and resonator-associated springs while maintaining nonlinearities in the internally coupled springs, and disregarding damping and electromechanical elements. The primary dynamic behavior emerges predominantly from the nonlinear internal coupling amidst resonators within a generally linear spring system, thereby facilitating a concentrated exploration into the effects and potential benefits of nonlinearity in inter-resonator springs.

The kinetic energy, symbolized by T , includes the dynamic activities of both the main chain and the resonators and is expressed as follows:

$$T = \frac{1}{2}m_m(\dot{u}_m^2 + \dot{u}_{m^+}^2) + \frac{1}{2}m_r(\dot{u}_r^2 + \dot{u}_{r^+}^2) \quad (2)$$

The potential energy, denoted by U , encapsulates the energy stored in various components of a mechanically coupled system: the main chain's linear springs, coupling springs between the chain and resonators, and notably, the nonlinear springs internally coupling the resonators provide a comprehensive view of energy distribution and interplay in a predominantly linear mechanical chain with specific nonlinear interactions.

$$U = \frac{1}{2}k_m[(u_{m^-} - u_m)^2 + (u_m - u_{m^+})^2 + (u_{m^+} - u_{m^{++}})^2] \\ + \frac{1}{2}k_r[(u_m - u_r)^2 + (u_{m^+} - u_{r^+})^2] \\ + \frac{1}{2}k_{c_1}(u_r - u_{r^+})^2 + \frac{1}{4}k_{c_2}(u_r - u_{r^+})^4 \quad (3)$$

Here, k_{c_1} and k_{c_2} serve as the linear and nonlinear coupling coefficients, respectively. While k_{c_1} facilitates a linear coupling between resonators, k_{c_2} introduces a bistable nonlinearity due to its fourth-order nature among the resonators. If both k_{c_1} and k_{c_2} are positive ($k_{c_1} > 0$ and $k_{c_2} > 0$), the system achieves a traditional monostable state, thereby circumventing the need to identify and linearize around a stable point. Opting for this strategy not only guarantees straightforward and stable system dynamics but also commonly serves to sidestep the intricacies encountered when navigating through bistable systems, especially in scenarios where $k_{c_1} < 0$ and $k_{c_2} > 0$. Utilizing the

Lagrangian formulation, and defining $z_r(t)$ as relative displacement between chain mass and resonator, the resonator's equation of motion yields

$$m_m \ddot{z}_r(t) + c_m(2\dot{z}_r(t) - \dot{z}_r(t) - \dot{z}_{r^+}(t)) + k_m(2z_r(t) - z_r(t) - z_{r^+}(t)) + k_r z_r(t) = f_{e_r} \quad (4)$$

$$m_m \ddot{z}_{r^+}(t) + c_m(2\dot{z}_{r^+}(t) - \dot{z}_r(t) - \dot{z}_{r^+}(t)) + k_m(2z_{r^+}(t) - z_r(t) - z_{r^+}(t)) + k_r z_{r^+}(t) = f_{e_{r^+}} \quad (5)$$

$$m_r \ddot{z}_r(t) + c_r \dot{z}_r(t) + k_r z_r(t) + k_{c_1}(z_r(t) - z_{r^+}(t)) + k_{c_2}(z_r(t) - z_{r^+}(t))^3 = f_{e_m} \quad (6)$$

$$m_r \ddot{z}_{r^+}(t) + c_r \dot{z}_{r^+}(t) + k_r z_{r^+}(t) - k_{c_1}(z_r(t) - z_{r^+}(t)) - k_{c_2}(z_r(t) - z_{r^+}(t))^3 = f_{e_{m^+}} \quad (7)$$

Here, m_m represents the mass of the main chain, and the coefficient k_m is the main chain's stiffness, interacting with the relative displacements between the resonator and its neighbors, while k_r characterizes the resonator's inherent stiffness. The f_{e_r} is the external excitation force on the primary mass chain. The resonator, with mass m_r , has a damping coefficient c_r and stiffness k_r . k_{c_1} is the linear coupling stiffness, while k_{c_2} is nonlinear. The forces f_{e_r} and $f_{e_{r^+}}$ indicate excitation on the primary mass chain, influenced by the resonator and internal connections. f_{e_m} and $f_{e_{m^+}}$ are the forcing on the resonators, sourced from the main chain mass and internal stiffness interactions.

2.4. Stability analysis for mechanical internally coupled metamaterial

The Jacobian matrix is commonly used to analyze the stability of equilibrium points for nonlinear systems. The idea is to linearize the nonlinear system around its equilibrium points and then analyze the stability of the resulting linear system. This provides insight into the local behavior of the nonlinear system around those points.

Considering equations (6) and (7) without the excitation force, the equilibrium points of the system can be ascertained. Setting the velocities \dot{z}_r and \dot{z}_{r^+} , along with the accelerations \ddot{z}_r and \ddot{z}_{r^+} , to zero provides the necessary conditions that define these equilibrium positions. The equilibrium points satisfy

$$\begin{aligned} k_r z_{r_0} + k_{c_1}(z_{r_0} - z_{r_0^+}) + k_{c_2}(z_{r_0} - z_{r_0^+})^3 &= 0 \\ k_r z_{r_0^+} - k_{c_1}(z_{r_0} - z_{r_0^+}) - k_{c_2}(z_{r_0} - z_{r_0^+})^3 &= 0 \end{aligned} \quad (8)$$

Introducing small perturbations around these equilibrium points results in the following expressions:

$$\begin{aligned} \delta z_r &= z_r - z_{r_0} \\ \delta z_{r^+} &= z_{r^+} - z_{r_0^+} \end{aligned} \quad (9)$$

Upon linearization of the equations of motion around the equilibrium, terms of higher order in δz_r and δz_{r^+} are neglected, leading to

$$\begin{aligned} m_r \delta \ddot{z}_r + c_r \delta \dot{z}_r + k_r \delta z_r + k_{c_1}(\delta z_r - \delta z_{r^+}) \\ + 3k_{c_2}(z_{r_0} - z_{r_0^+})^2 (\delta z_r - \delta z_{r^+}) &= 0 \end{aligned} \quad (10)$$

$$\begin{aligned} m_r \delta \ddot{z}_{r^+} + c_r \delta \dot{z}_{r^+} + k_r \delta z_{r^+} - k_{c_1}(\delta z_r - \delta z_{r^+}) \\ - 3k_{c_2}(z_{r_0} - z_{r_0^+})^2 (\delta z_r - \delta z_{r^+}) &= 0 \end{aligned} \quad (11)$$

A state vector is introduced to convert the second-order system into a system of first order:

$$X = \begin{bmatrix} \delta z_r \\ \delta z_{r^+} \\ \delta \dot{z}_r \\ \delta \dot{z}_{r^+} \end{bmatrix} \quad (12)$$

Differentiating the state vector yields

$$\dot{X} = \begin{bmatrix} \delta \dot{z}_r \\ \delta \dot{z}_{r^+} \\ \delta \ddot{z}_r \\ \delta \ddot{z}_{r^+} \end{bmatrix} \quad (13)$$

The objective is to represent \dot{X} in the form AX , where A is a matrix constructed from the system parameters and possibly the equilibrium point. The matrix A is determined by linearizing the equations of motion. The eigenvalues of A indicate the stability of the system around the equilibrium.

The eigenvalue for the nonlinear internally coupled resonators is determined by equations (14) and (15):

$$\lambda_{1,3} = -\frac{c_r \pm \sqrt{c_r^2 - 4k_r m_r}}{2m_r} \quad (14)$$

$$\lambda_{2,4} = -\frac{1}{2m_r} (c_r \pm \sqrt{c_r^2 - 4m_r k_r - 8m_r (k_{c_1} + 3k_{c_2}(\delta z_r - \delta z_{r^+})^2)}) \quad (15)$$

By omitting the nonlinear term k_{c_2} , the system transitions to a linear internally coupled resonator. This exclusion simplifies the stability analysis by removing the nonlinear component. Consequently, the system's behavior is analyzed linearly around its equilibrium point. After this simplification, the governing equation of motion becomes

$$\lambda_{1,3} = -\frac{c_r \pm \sqrt{c_r^2 - 4k_r m_r}}{2m_r} \quad (16)$$

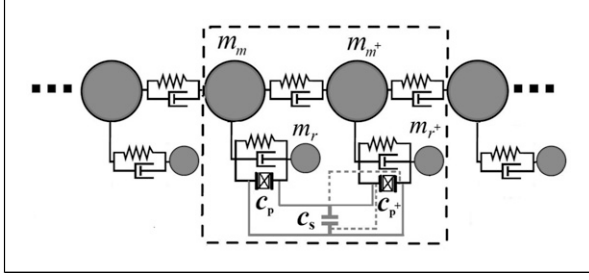


Figure 2. Internally coupled system with electrical shunt circuit: Forward (dashed line) and reverse (solid line) capacitance shunting configurations.

$$\lambda_{2,4} = -\frac{c_r \pm \sqrt{c_r^2 - 4m_r(k_r + 2k_c)}}{2m_r} \quad (17)$$

Stability scenarios for internally coupled systems:

2.4.1. Nonlinear systems:

Case 1: For $c_r^2 - 4k_r m_r < 0$, $\lambda_{1,3}$ imply a stable focus.

Case 2: With $c_r^2 - 4k_r m_r > 0$ and all positive parameters, λ_1 and λ_3 ensure stability.

Case 3: Sign of $\lambda_{2,4}$ depends on term magnitudes and c_r .

Case 4: $c_r^2 - 4k_r m_r - 8m_r(k_{c1} + 3k_{c2}(\delta z_r - \delta z_{r+})^2) < 0$ denotes stability.

2.4.2. Linear systems:

Case 1: For $c_r^2 - 4k_r m_r < 0$, $\lambda_{1,3}$ indicate a stable focus.

Case 2: With $c_r^2 - 4k_r m_r > 0$, signs of λ_1 and λ_3 are determined by c_r .

Case 3: In $c_r^2 - 4k_r m_r - 8k_c m_r > 0$, stability relies on signs of λ_2 and λ_4 .

Case 4: Condition $c_r^2 - 4k_r m_r - 8k_c m_r < 0$ signals stability.

2.5. Electromechanical resonators with internal coupling via shunt capacitance circuit technique

In the preceding section, the metamaterial with internal resonator coupling was examined. Due to challenges in constructing and instructing the internal spring, especially when aiming for negative stiffness, an alternative is to utilize an electrical shunt circuit, specifically a prototype capacitance, offering behavior similar to the mechanically internally coupled resonator.

In this section, the shunt capacitance circuit technique is employed to model a two-degree-of-freedom electrical system with internal coupling, as illustrated in Figure 2. In this scenario, capacitance is incorporated as a key component instead of utilizing the resistance (R) as load.

Figure 2 illustrates the forward and reverse shunt circuit setups. The forward pairs the top and bottom surfaces of piezoelectric transducers, whereas the reverse opposes

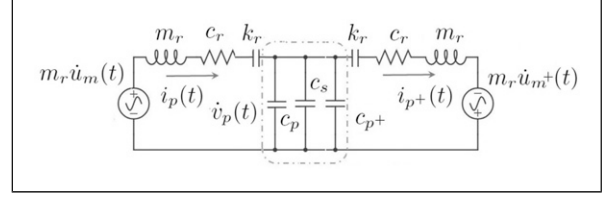


Figure 3. Electrical analog of unit cell resonators with capacitance shunt circuit via impedance method.

them. Both configurations use a parallel capacitor and yield similar analytical conclusions, with the only difference being a sign change in the coupling stiffness. Despite their similarities, this study primarily focuses on the reverse setup due to its straightforward mechanical interpretation when no external capacitance is present. In terms of capacitance, positive values lower voltage during current discharge, while negative ones raise it. Drawing from the impedance analogy, the segments LRC and LRC^+ correspond to resonators m_r, c_r, k_r and $(m_r, c_r, k_r)^+$, as displayed in Figure 3.

The voltage across the capacitance reflects force interactions between resonators. Current and charge shifts denote velocity and displacement variations. Essentially, the capacitor acts as a coupling spring, its stiffness determined by the capacitance sign. In the reverse setup for piezoelectric transducers, voltages possess equal magnitude but opposite directions, influenced by the current in the parallel capacitance c_s , as

$$\frac{1}{c_s} \int (i_p(t) - i_{p+}(t)) dt = v_p(t) \quad (18)$$

The design uses an internal shunt capacitance, tuned to act as a negative capacitor, to boost resonator performance and strengthen adjacent resonator coupling. Given identical properties for all resonators, including stiffness, damping, and mass, the governing equations for the motion of two resonators within a unit cell, as seen in Figure 2, are

$$m_r \ddot{z}_r(t) + c_r \dot{z}_r(t) + k_r z_r(t) + \theta_r v_p(t) = m_r \ddot{u}_m(t) \quad (19)$$

$$m_r \ddot{z}_{r+}(t) + c_r \dot{z}_{r+}(t) + k_r z_{r+}(t) + \theta_{r+} v_{p+}(t) = m_r \ddot{u}_{m+}(t) \quad (20)$$

Relative displacements of the resonators to the main structure can be defined as $z_r = u_m - u_r$ and $z_{r+} = u_{m+} - u_{r+}$. The coefficients θ_r and θ_{r+} represent electromechanical coupling, with associated voltages $v_p(t)$ and $v_{p+}(t)$. The corresponding electrical equations for the transducers are

$$c_p \dot{v}_p(t) + i_p(t) - \theta_r \dot{z}_r(t) = 0 \quad (21)$$

$$c_p \dot{v}_{p^+}(t) + i_{p^+}(t) - \theta_r \dot{z}_{r^+}(t) = 0 \quad (22)$$

By substituting equation (18) into equations (21) and (22), expressions for currents $i_p(t)$ and $i_{p^+}(t)$ in the loops are derived as

$$i_p(t) = \frac{c_{p^+} \theta_r \dot{z}_r + c_p \theta_{r^+} \dot{z}_{r^+} + c_s \theta_r \dot{z}_r}{c_p + c_{p^+} + c_s} \quad (23)$$

$$i_{p^+}(t) = \frac{c_{p^+} \theta_r \dot{z}_r + c_p \theta_{r^+} \dot{z}_{r^+} + c_s \theta_{r^+} \dot{z}_{r^+}}{c_p + c_{p^+} + c_s} \quad (24)$$

Substituting equation (23) and equation (24) into equation (18) and integrating with respect to time for zero initial condition yields

$$v_p(t) = \frac{(\theta_r z_r - \theta_{r^+} z_{r^+})}{c_p + c_{p^+} + c_s} \quad (25)$$

$$v_{p^+}(t) = -\frac{(\theta_r z_r - \theta_{r^+} z_{r^+})}{c_p + c_{p^+} + c_s} \quad (26)$$

Substituting equation (25) and equation (26) into equation (19) and equation (20) yields the following expressions:

$$\begin{aligned} m_r \ddot{z}_r(t) + c_r \dot{z}_r(t) + k_r z_r(t) + k_{s_1} z_r(t) \\ - k_{s_2} z_{r^+}(t) = m_r \ddot{u}_m(t) \end{aligned} \quad (27)$$

$$\begin{aligned} m_r \ddot{z}_{r^+}(t) + c_r \dot{z}_{r^+}(t) + k_r z_{r^+}(t) \\ - k_{s_2} z_r(t) + k_{s_3} z_{r^+}(t) = m_r \ddot{u}_{m^+}(t) \end{aligned} \quad (28)$$

where

$$k_{s_1} = \frac{\theta_r^2}{c_p + c_{p^+} + c_s} \quad (29)$$

$$k_{s_2} = \frac{\theta_r \theta_{r^+}}{c_p + c_{p^+} + c_s} \quad (30)$$

$$k_{s_3} = \frac{\theta_{r^+}^2}{c_p + c_{p^+} + c_s} \quad (31)$$

For identical electromechanical couplings and after substituting the relevant equations into equation (18), the integrated result yields the following condensed motion equations:

$$\begin{aligned} m_r \ddot{z}_r(t) + c_r \dot{z}_r(t) + k_r z_r(t) \\ + k_s (z_r(t) - z_{r^+}(t)) = m_r \ddot{u}_m(t) \end{aligned} \quad (32)$$

$$\begin{aligned} m_r \ddot{z}_{r^+}(t) + c_r \dot{z}_{r^+}(t) + k_r z_{r^+}(t) \\ - k_s (z_r(t) - z_{r^+}(t)) = m_r \ddot{u}_{m^+}(t) \end{aligned} \quad (33)$$

where

$$k_s = \frac{\theta_r^2}{c_p + c_{p^+} + c_s} \quad (34)$$

2.6. Stability analysis for electromechanical internally coupled resonators via shunt capacitance

The stability of the system hinges on k_s , denoting electromechanical coupling through the shunt circuit. Instability might arise with negative shunt capacitance. For the dual-resonator setup, stability is gauged by linearizing its equations of motion and inspecting the eigenvalues of the Jacobian matrix. A system is stable if all its eigenvalues possess negative real parts. By analyzing the Jacobian matrix derived from linearizing around equilibrium, we discern system behavior. The system remains stable with all eigenvalues in the left-half complex plane. Achieving negative stiffness necessitates k_{s_1} , k_{s_2} , and k_{s_3} to be negative. Uniform electromechanical coupling demands $k_s < 0$.

For a system with positive electromechanical coupling, achieving a negative k_s necessitates the combined c_p and c_s to be negative, indicating a need for negative capacitance. This can be realized using active circuits with operational amplifiers or ferroelectric capacitors. However, this introduces challenges such as potential destabilization. Ensuring system stability, especially with negative capacitance, is paramount, often verified using Jacobian analysis. Mathematically, a corresponding linear system is expressed as

$$m\ddot{z}(t) + c\dot{z}(t) + kz(t) = f(t) \quad (35)$$

with

$$z(t) = \begin{bmatrix} z_r(t) \\ z_{r^+}(t) \end{bmatrix}$$

The system's stability is influenced by the eigenvalues of the Jacobian matrix, determined by equation (36). These eigenvalues are shaped by the damping coefficient c_r and shunt coefficients k_{s_1} , k_{s_2} , and k_{s_3} . While damping can promote stability, spring coefficients introduce potential oscillations. The interplay of couplings k_{s_1} , k_{s_3} , and k_{s_2} deeply impacts the system dynamics. A system is stable when all eigenvalues have negative real parts. If

$$\lambda = \frac{-c_r \pm \sqrt{c_r^2 - 2k_{s_1}m_r - 2k_{s_3}m_r - 4k_r m_r \pm 2m_r \sqrt{k_{s_1}^2 - 2k_{s_1}k_{s_3} + 4k_{s_2}^2 + k_{s_3}^2}}}{2m_r} \quad (36)$$

Table 1. Defined parameters for the piezoelectric model.

Parameter	Value
Mass of main chain (m_m)	0.056 kg
Mass of resonator (m_r)	0.0336 kg
Spring constant of main chain (k_m)	150 N/m
Spring constant of resonator (k_r)	129.6 N/m
Damping coefficient of main chain (c_m)	0.0464 Ns/m
Damping coefficient of resonator (c_r)	0.0334 Ns/m
Piezoelectric capacitance (c_p)	1.5 mF(C/m)
Adjacent resonator's capacitance (c_{p^+})	1.2 mF(C/m)
Electromechanical coupling coefficient (θ_r)	0.25 N/V
Adjacent electromechanical coupling (θ_{r^+})	0.2 N/V
Linear coupling coefficient (k_{c_1})	198 (-20) N/m
Nonlinear coupling coefficient (k_{c_2})	2386 (880) N/m ³
Shunt capacitance (c_s)	-7.9 mF(C/m)
Internal resistance (R)	500 Ω

the discriminant is negative, oscillatory behaviors emerge.

Notably, the real component of λ , defined as $-c_r/2m_r$, predisposes the system to stability, but further analysis is essential for a full understanding.

$$a = c_r^2 - 2k_{s_1}m_r - 2k_{s_3}m_r - 4k_r m_r \quad (37)$$

$$b = 2m_r \sqrt{k_{s_1}^2 - 2k_{s_1}k_{s_3} + 4k_{s_2}^2 + k_{s_3}^2} \quad (38)$$

Case 1: $a < 0$ and $b < 0$, the system is stable if $|a| > |b|$.

Case 2: $a > 0$ and $b > 0$, the system is stable if $a < b$.

Case 3: $a > 0$ and $b < 0$, stability would need to be ascertained by calculating the actual values and verifying the sign of λ . The system can lead to an unstable region.

Case 4: $a < 0$ and $b > 0$, the system is stable if $|a| > |b|$.

Case 5: $a = 0$ or $b = 0$, the system is stable.

For a marginally stable system, damping is typically disregarded to establish boundaries of stability. As per equation (39), when the system's eigenvalues are purely imaginary, it denotes a marginal stability condition. This equation delineates constraints on the stiffness coefficients k_r and k_s , defining the threshold between stable and unstable regimes.

$$2k_r > -k_{s_1} - k_{s_3} - \sqrt{k_{s_1}^2 - 2k_{s_1}k_{s_3} + 4k_{s_2}^2 + k_{s_3}^2} \quad (39)$$

The associated eigenvalues, representing the system's characteristic frequencies, are given by

$$\lambda = \pm \frac{1}{\sqrt{2}} \sqrt{\frac{-\left(2k_r + k_{s_1} + k_{s_3} \pm \sqrt{k_{s_1}^2 - 2k_{s_1}k_{s_3} + 4k_{s_2}^2 + k_{s_3}^2}\right)}{m_r}} \quad (40)$$

To identify criteria for c_s that ensures a negative equivalent stiffness, equations (29), (30), and (31) are substituted into (37) and (38). The derived expressions are then analyzed to determine the conditions for c_s that satisfy the stability conditions

$$a - b < 0 \quad (41)$$

$$|a| > |b| \quad (42)$$

Substituting a and b into equation (41) for the stability condition of $a - b < 0$ yields

$$c_r^2 - 4k_r m_r < 2m_r \left(\frac{\theta_r^2 + \theta_{r^+}^2 + \sqrt{\theta_r^4 + 2\theta_r^2\theta_{r^+}^2 + \theta_{r^+}^4}}{c_p + c_{p^+} + c_s} \right) \quad (43)$$

Taking into account the absolute values in equation (42), it becomes imperative to explore two scenarios due to the potential positivity or negativity of both a and b .

$$|c_r^2 - 4k_r m_r| > \left| 2m_r \frac{\sqrt{\theta_r^4 + 2\theta_r^2\theta_{r^+}^2 + \theta_{r^+}^4}}{c_p + c_{p^+} + c_s} \right| \quad (44)$$

The inequalities (44) and (43) should be satisfied for stability, and c_s appears in the denominator of the fractions in these expressions, implying that as c_s changes, the values of these expressions will alter, potentially changing the sign of the inequalities. To derive explicit criteria, one could further manipulate these expressions or, depending on the specific application or system, analyze them numerically by substituting values of other parameters (c_r, k_r, m_r , etc.) to explore how varying c_s affects the system's stability. Solving for c_s results in

$$c_s > \frac{2m_r \left(\theta_r^2 + \theta_{r^+}^2 + \sqrt{\theta_r^4 + 2\theta_r^2\theta_{r^+}^2 + \theta_{r^+}^4} \right)}{c_r^2 - 4k_r m_r} - c_p - c_{p^+} \quad (45)$$

In the case of identical electromechanical coupling, and capacitance, the criteria for c_s can be simplified as follows:

$$c_s > \frac{8m_r \theta_r^2}{c_r^2 - 4k_r m_r} - 2c_p \quad (46)$$

In the scenario devoid of damping, the eigenvalues of the system, representing its characteristic roots, are provided as follows:

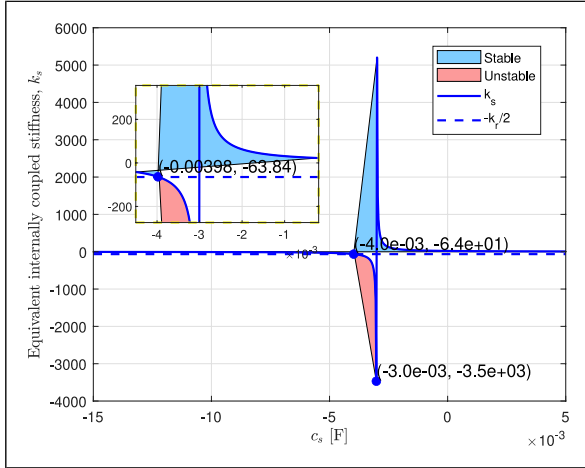


Figure 4. Stability map for the electromechanical lumped system: interplay between equivalent stiffness k_s and shunt capacitance c_s . Parameters: $n = 4$, $m_m = 56$ g, $m_r = 33.6$ g, $k_m = 150$ N/m, $k_r = 129.6$ N/m, $\theta = 0.25$ N/V, $R = 500$ Ω , and $c_p = 1.5 \times 10^{-3}$ F.

$$\lambda_{1,2} = \pm \frac{\sqrt{-k_r m_r}}{m_r} \quad (47)$$

$$\lambda_{3,4} = \pm \frac{\sqrt{-m_r(k_r + 2k_s)}}{m_r}$$

The system's stability is defined by the real parts of its eigenvalues. When $k_r + 2k_s > 0$, the system exhibits marginal stability, oscillating continuously without decay or growth. However, if $k_r + 2k_s < 0$, the system has both positive and negative eigenvalues, indicating instability. This highlights the critical relationship between the resonator's spring constant and the shunt capacitance stiffness (k_s). If the feedback from the shunt is overly negative, it can destabilize the system. In most applications, full stability is preferred over marginal stability. The stability criterion for c_s is

$$c_s > - \left(\frac{2\theta_r^2}{k_r} + 2c_p \right) \quad (48)$$

In contrast to purely mechanical internally coupled resonators, electromechanical shunt capacitance circuits provide benefits over solely mechanical resonators by allowing easy adjustments for negative stiffness. The system's flexibility is further amplified by altering parameters like c_p , c_{p+} , θ_r , and θ_{r+} , enabling advanced system behaviors and improved dynamic control.

3. Simulation analysis and discussion

The simulation model used in this study has investigated both mechanical and electromechanical dynamics, with a focus on piezoelectric components'

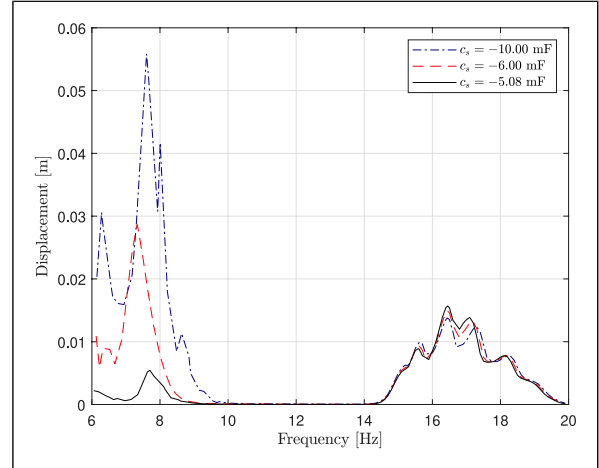


Figure 5. Transmittance comparison of electrical internally coupling with shunt circuit for $\theta = 0.25$ and $c_p = 1.5$ mF, demonstrating the impact of an equivalent negative stiffness of $k_s = -30$.

key parameters as depicted in Table 1. Differential equations representing the system were solved using the fourth-order Runge–Kutta method. The garnered results have offered profound insights into system performance aspects, notably vibration control, energy capture, and power efficiency.

The model revealed four wavelengths (λ) for creating distinct dispersion curves stemming from the presence of four inertias within a unit cell, suggesting the potential for enhanced band gaps in internally coupled metamaterials as opposed to conventional ones. While our research concentrated on a select frequency range to delineate the variances between mechanical and electromechanical internal coupling, the broader implications of all band gaps across the entire frequency spectrum remain an open field for future exploration.

Incorporating real-world scenarios, our research encapsulates applications that harness high-capacitance piezoelectric materials. These include pedestrian energy-harvesting floor tiles in airports, vibration dampers in industrial machinery, structural health monitors for bridges and buildings, energy-recapturing systems in automotive suspensions, and self-charging phone cases. These case studies demonstrate the practical engineering scenarios where our research can be applied, emphasizing the transformative impact of our findings on sustainable engineering design and operation.

3.1. Shunt capacitance influence on system stability and energy-harvesting efficiency

Figure 4 illustrates the relationship from equation (48). For system stability, the equivalent internal coupling stiffness k_s should exceed $k_s = -k_r/2$. The figure illustrates the

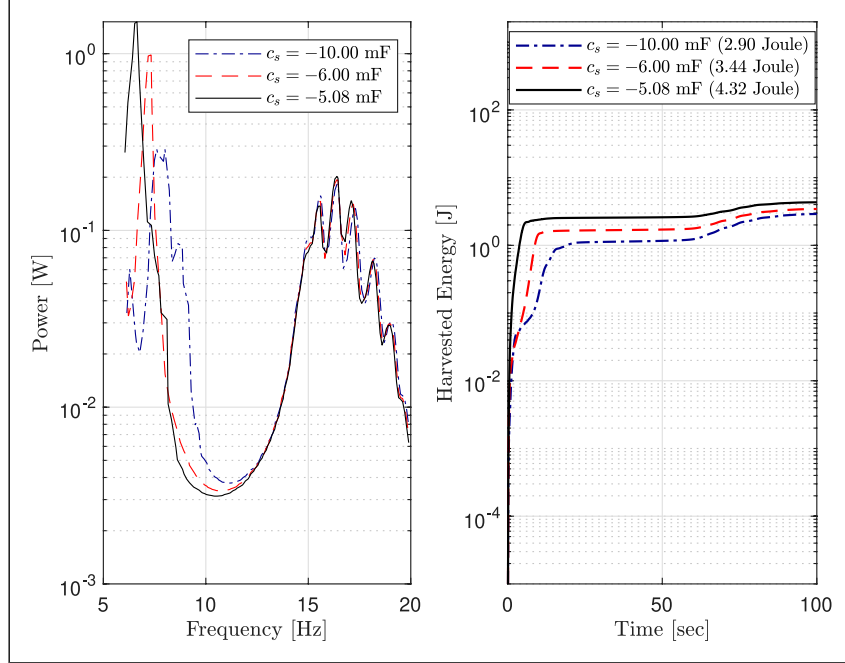


Figure 6. Power and energy harvesting across various shunt capacitances with $\theta = 0.25$ and $c_p = 1.5$ mF.

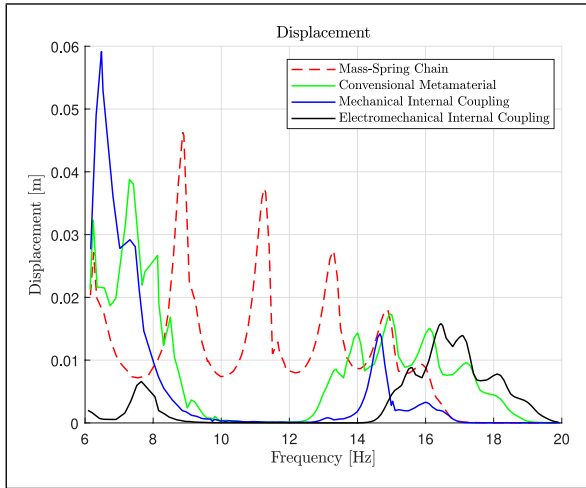


Figure 7. Frequency response analysis: comparative displacement profiles of mechanical, conventional metamaterial, and electromechanical internally coupled systems based on parameters in Table 1.

relationship between k_s and shunt capacitance c_s . The light blue area denotes system stability, while the reddish color signifies instability. Given the parameters, stability is maintained for c_s values from negative infinity to about -0.004 F and from around -0.003 F to positive infinity. However, there's a brief unstable period in between. A zoomed-in view highlights the crucial c_s values where the system behavior changes.

In the study of energy-harvesting systems, understanding the behavior of different parameters is essential for optimization. From the simulations, key insights have emerged. Figure 6 presents the harvested power and energy across a range of shunt capacitances. It clearly underscores the influential role of shunt capacitance on the system's overall efficiency.

A pivotal observation made from the results is the superiority of electrical internal coupling via shunt circuits in terms of tunability. Specifically, electrical coupling seems to allow for easier tuning of the band gap compared to its mechanical counterpart. This is evident in Figures 5 and 6, where the chosen shunt capacitor facilitates a band gap at a notably lower frequency in comparison to a mechanically internally coupled system, as illustrated in Figure 7.

Selecting a shunt capacitance of $c_s = -5.08$ mF results in an equivalent stiffness of $k_s = -30$. This specific choice not only introduces an equivalent negative stiffness into the system, enhancing energy-harvesting capabilities across varied frequency spectrums, but also facilitates the creation of a band gap at a lower frequency (see Figure 5). Compared to mechanical internally coupled resonators, this allows for more flexible and straightforward tuning of the band gap across different frequencies.

3.2. Electromechanical internally coupled resonators

Figure 7 illustrates the displacement response across different frequency ranges for four distinct systems: mass–

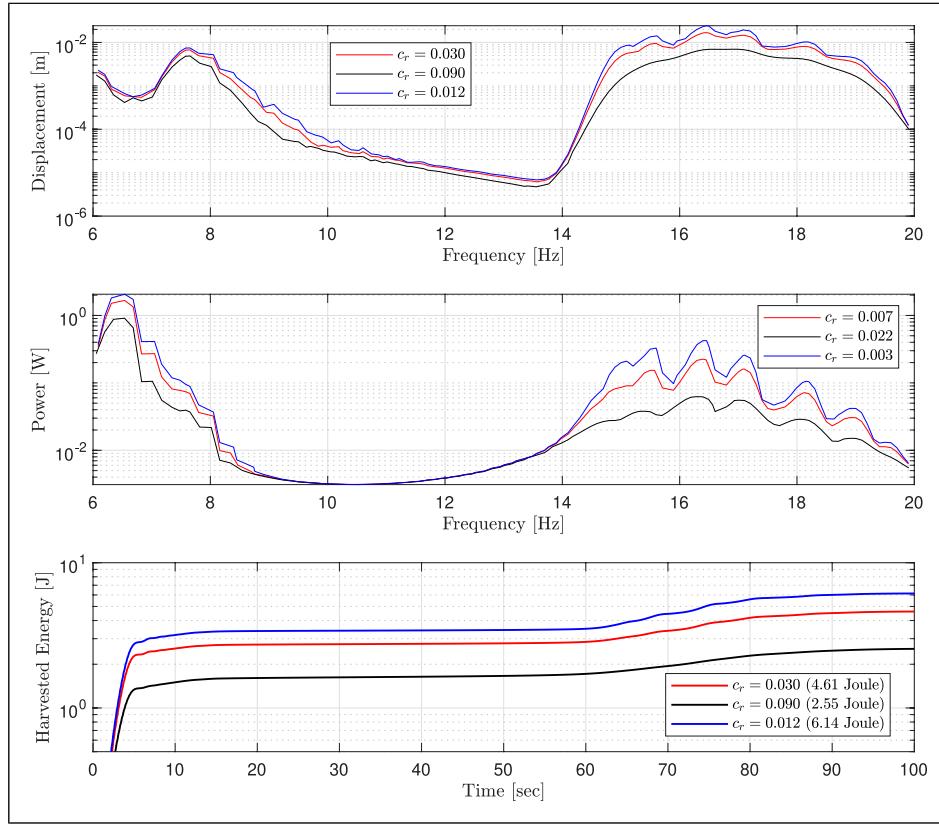


Figure 8. Frequency response showcasing the influence of varying resonator damping coefficients (c_r) on displacement, power generation, and accumulated harvested energy. A higher c_r reveals a smoothed response with broader bandwidth but reduced peak values.

spring chain, conventional metamaterial, mechanical internal coupling, and electromechanical internal coupling. The mechanical internally coupled system has a dominant response at around 7 Hz, peaking at a displacement of approximately 0.06 m, but its effectiveness drops beyond 12 Hz. In contrast, the conventional metamaterial with linear resonators responds at multiple frequencies, especially around 12 Hz and 14 Hz. Both the mechanical and electromechanical internal coupling systems exhibit intricate frequency responses, with the latter demonstrating a wider range of resonances. Displacement magnitudes suggest potential energy-harvesting capabilities, with greater displacements indicating more energy conversion potential. Notably, while the electromechanical system might display a reduced displacement compared to its purely mechanical counterpart, its broader frequency response makes it versatile, though its energy-harvesting efficacy needs further examination as indicated in Figure 9.

From Figures 8 and 9, the damping coefficients of mass chain c_m and resonator c_r alter displacement and power generation profiles across frequencies. A higher damping smoothens the response, lessening peak displacements while broadening the frequency response. This results in decreased peak power but an enhanced ability to harvest

energy across a wider frequency range. Observations show that a steeper curve corresponds to more energy harvested over time with a higher c_r . For this case study, the electromechanical parameters, $\theta = 0.25$ N/V, internal resistance $R = 500 \Omega$, and shunt capacitance $c_s = -5$ mF are selected. As seen in Figure 8, different values of c_r lead to varied displacement, power, and energy profiles. It directly affects the sharpness of the resonance peak and the bandwidth of the system's frequency response. A high c_r broadens the response, suitable for environments with varied frequencies but at the cost of peak performance.

In comparing the displacements from Figures 8 and 9, it's evident that the behaviors of c_m and c_r diverge. Specifically, c_m prominently impacts the system's transient response and settling time. Notably, even with piezoelements on the resonator, increased main chain damping (c_m) leads to reduced energy harvesting. This underlines the intricate dynamics between resonator and mass chain damping in energy-harvesting systems.

Figure 10 shows the displacement response of nonlinear mechanical internal coupling resonators over a frequency sweep. The plot contrasts the displacement during upward and downward frequency sweeps, revealing the nonlinear behavior and hinting at the presence of bifurcation around

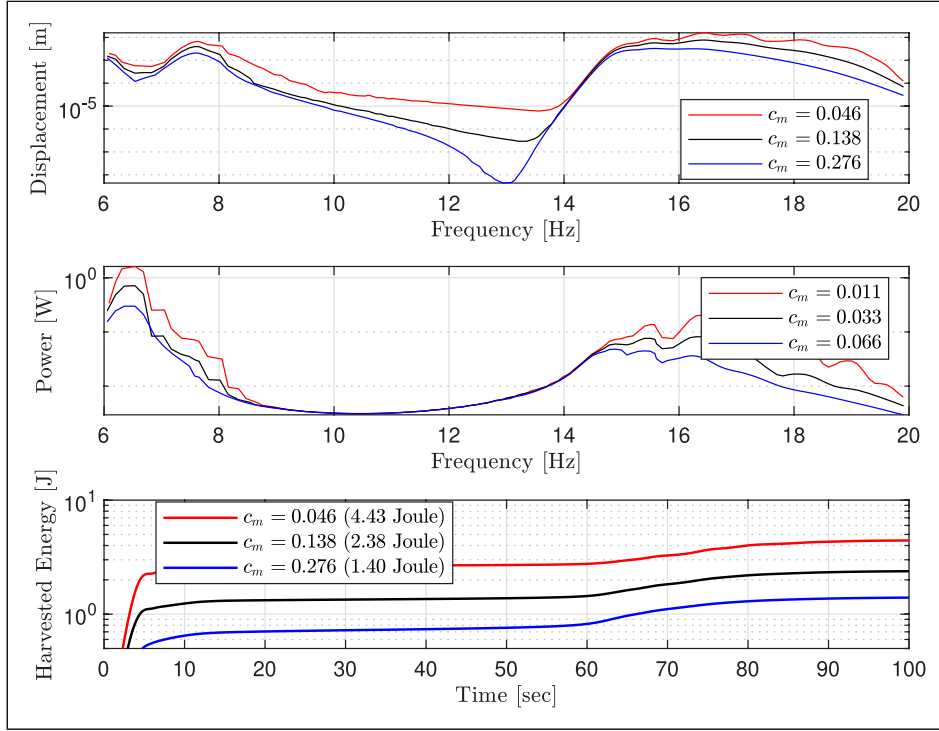


Figure 9. Displacement profiles as influenced by the mass chain damping (c_m). The transient response and settling time of the system are notably affected by c_m . The plot underscores the reduced energy harvesting as c_m increases, despite the presence of piezoelements on the resonator.

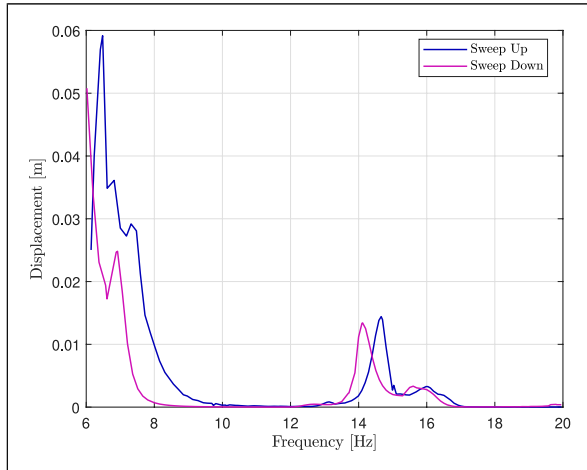


Figure 10. Displacement response of nonlinear mechanical internal coupling resonators over a frequency sweep, with linear coupling coefficient $k_{c1} = 198 \text{ N/m}$ and nonlinear coupling coefficient $k_{c2} = 2386 \text{ N/m}^3$.

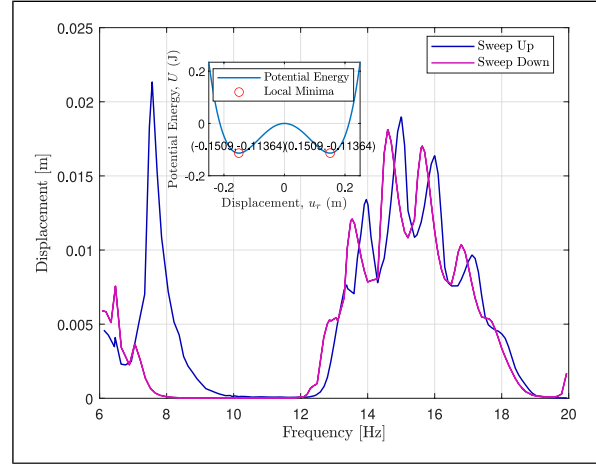


Figure 11. Displacement response of bistable nonlinear mechanical internal coupling resonators: linear coupling coefficient $k_{c1} = -20 \text{ N/m}$ and nonlinear coupling coefficient $k_{c2} = 880 \text{ N/m}^3$. Inset: Resonator’s potential energy profile for the specified coupling parameters.

15 Hz. This nonlinearity is influenced by the linear coupling coefficient (k_{c1}) of 198 N/m and the nonlinear coupling coefficient (k_{c2}) of 2386 N/m^3 . The continuous nature of the sweep and the plot’s point-connecting methodology give the bifurcation its observed shape.

Figure 11 illustrates bistable-type nonlinear mechanical resonators with internal coupling. The parameters employed include linear coupling coefficient (k_{c1}) -20 N/m and nonlinear coupling coefficient (k_{c2}) $0.88e3 \text{ N/m}^3$. The graph represents the resonator’s

potential energy in relation to displacement. It emphasizes the unstable point of origin with negative stiffness. It's worth noting that the system's dynamics are highly sensitive to the value of k_{c_2} . Similar to Figure 10, in the frequency range of 14–16 Hz, bifurcation is observed. The non-coinciding sweep up/down traces indicates the presence of hysteresis, highlighting the system's nonlinear behavior.

The inset plot within the main figure shows a graph of potential energy against displacement. This highlights the energy state of the system for different displacements. The presence of multiple local minima indicates that the system can occupy multiple stable states for specific energy levels. This behavior indicates multi-stability in the system, especially if the resonators encounter large fluctuation range. The peaks, especially those around 8 Hz and 15 Hz, show clear discrepancies between the sweep up/down traces. This difference highlights the system's nonlinear hysteresis behavior. Beyond the 16 Hz mark, multiple peaks and valleys suggest that the system has several resonance frequencies or harmonics. These characteristics can arise due to the interplay of the system parameters and nonlinearities.

Leveraging bistability in phononic media can profoundly alter the wave response within band gaps via supra-transmission, a phenomenon documented in bistable periodic chains both with and without resonators (Frazier and Kochmann, 2017), as well as in metastable modular meta-structures (Wu and Wang, 2019). Nonetheless, in this context, the parameters of the bistable system are deliberately chosen to operate within a confined frequency range, aiming to exclusively simulate the system akin to negative stiffness found in electromechanical systems utilizing shunt circuits.

To enhance the validity of these findings, supplementary numerical simulations were executed, integrating decreased piezoelectric capacitance values. Specifically, c_p and c_{p+} were adjusted to 800 nF. With other parameters kept constant (k_r , m_r , and c_r), and the electromechanical coupling coefficients θ_r and θ_{r+} set at 0.01 N/V, these simulations were crucial in reinforcing the robustness of the study's findings. Stability analysis revealed that, for system stability, the shunt capacitance c_s must exceed $-3.48 \mu\text{F}$. This criterion was tested with values such as $-1.5 \mu\text{F}$, -200 nF , and -10 pF . Conducted within a pragmatic range of piezoelectric capacitance, these simulations not only confirmed the initial results but also underscored the model's practical applicability and relevance. The insights derived from this extended simulation effort are integrated into the study, ensuring that the conclusions drawn are firmly rooted in realistic engineering contexts.

4. Conclusion

In conclusion, this investigation into the dynamics of internally coupled resonators within metamaterial systems has underscored the critical balance between resonator stiffness

and shunt capacitance stiffness, k_s . Our stability analysis reveals that excessive negative feedback can lead to system instability, thus necessitating careful parameter tuning.

The simulations have demonstrated the significant advantages of electromechanical shunt capacitance circuits, notably in adjusting negative stiffness and facilitating lower operational frequency band gaps. These insights are invaluable for understanding system efficiency and the effectiveness of electrical internal coupling in energy harvesting. Furthermore, the study of nonlinear characteristics like bifurcation and hysteresis in resonators paves the way for innovative energy-harvesting device designs.

To further validate these findings, additional numerical simulations were conducted with lower piezoelectric capacitance values. This extension of the simulation framework reinforced the robustness of the initial results and confirmed the model's practical applicability and relevance in realistic scenarios.

The applications of high-capacitance (millifarad-level) piezoelectric materials span various sectors. They enable energy-harvesting floor tiles in high-traffic areas like airports, vibration damping in industrial machinery, continuous structural monitoring in buildings and bridges, energy recapture in vehicle suspensions, self-charging solutions for personal electronics, and long-lasting power sources for wearable health monitors. These applications underscore the significant potential and real-world impact of advanced piezoelectric materials in energy harvesting and sustainability.

Guidance for augmenting the capacitance of piezoelectric materials involves selecting materials such as PZT or polymer-based composites with higher dielectric constants, optimizing the geometry of piezoelectric elements, employing multi-layer structures, and connecting multiple capacitors in parallel. These strategies cumulatively increase the overall capacitance available for energy harvesting and other applications.

The key contributions of this research include the analysis of band gaps and energy-harvesting capabilities within linear and nonlinear coupled resonators in lumped systems, a novel stability analysis approach for these systems, and insights into optimizing metamaterials for energy harvesting. A significant discovery is the identification of enhanced band gaps in internally coupled resonators. Our work demonstrates the advantages of electromechanical shunt circuits in fine-tuning band gaps for optimized performance, marking significant steps forward in harnessing the potential of piezoelectric materials for sustainable energy solutions.

5. Future works

This study offers significant insights into the stability and energy harvesting capabilities of internally coupled resonators within lumped parameter systems. Looking ahead, several suggestions for future research emerge: Firstly, there

is a clear necessity for detailed investigation aimed at optimizing coupling parameters, such as capacitance values and nonlinear coefficients, with the aim of maximizing energy harvesting efficiency and bolstering system stability. Furthermore, extending our analysis to encompass networks of internally coupled resonators within distributed parameter systems will be invaluable. Such exploration is critical for deciphering how interactions among multiple resonators affect their collective stability and energy harvesting efficiency. Additionally, the exploration of adaptive control techniques presents an exciting frontier. By dynamically adjusting the coupling parameters in response to fluctuating system conditions, these techniques promise to significantly enhance the adaptability and performance of resonator systems.

Declaration of conflicting interests

The author(s) declared no potential conflicts of interest with respect to the research, authorship, and/or publication of this article.

Funding

The author(s) disclosed receipt of the following financial support for the research, authorship, and/or publication of this article: This work was supported by the European Union's Horizon Europe research and innovation programme under the grant agreement No. 101120657, project ENFIELD (European Lighthouse to Manifest Trustworthy and Green AI), by the Estonian Research Council through the grant PRG658, and by the Estonian Centre of Excellence in Energy Efficiency, ENER (grant TK230) funded by the Estonian Ministry of Education and Research.

ORCID iDs

H Alimohammadi  <https://orcid.org/0000-0002-8867-8988>

K Vassiljeva  <https://orcid.org/0000-0002-4178-1267>

S H HosseinNia  <https://orcid.org/0000-0002-7475-4628>

E Petlenkov  <https://orcid.org/0000-0003-2167-6280>

References

- Chatziathanasiou GM, Chrysochoidis NA and Saravanos DA (2022) A semi-active shunted piezoelectric tuned mass damper for robust vibration control. *Journal of Vibration and Control* 28(21-22): 2969–2983.
- Chaunsali R, Xu H, Yang J, et al. (2021) Stability of topological edge states under strong nonlinear effects. *Physical Review B* 103(2): 024106.
- Fang X, Wen J, Bonello B, et al. (2017) Wave propagation in one-dimensional nonlinear acoustic metamaterials. *New Journal of Physics* 19(5): 053007.
- Frazier MJ and Kochmann DM (2017) Band gap transmission in periodic bistable mechanical systems. *Journal of Sound and Vibration* 388: 315–326.
- Fronk MD and Leamy MJ (2017) Higher-order dispersion, stability, and waveform invariance in nonlinear monoatomic and diatomic systems. *Journal of Vibration and Acoustics* 139(5): 051003.
- Fronk MD and Leamy MJ (2019) Direction-dependent invariant waveforms and stability in two-dimensional, weakly nonlinear lattices. *Journal of Sound and Vibration* 447: 137–154.
- Hoogeboom C, Man Y, Boechler N, et al. (2013) Hysteresis loops and multi-stability: from periodic orbits to chaotic dynamics (and back) in diatomic granular crystals. *Europhysics Letters* 101(4): 44003.
- Hu G, Tang L, Banerjee A, et al. (2017) Metastucture with piezoelectric element for simultaneous vibration suppression and energy harvesting. *Journal of Vibration and Acoustics* 139(1): 011012.
- Hu G, Tang L and Das R (2018) Internally coupled metamaterial beam for simultaneous vibration suppression and low frequency energy harvesting. *Journal of Applied Physics* 123(5).
- Lefeuve E, Badel A, Richard C, et al. (2005) Piezoelectric energy harvesting device optimization by synchronous electric charge extraction. *Journal of Intelligent Material Systems and Structures* 16(10): 865–876.
- Li X, Yu Z, Iizuka H, et al. (2023) Observation of an exceptional point with an Ir-shunted resonator. *Mechanical Systems and Signal Processing* 196: 110297.
- Liu Y, Yang J, Yi X, et al. (2022) Enhanced vibration suppression using diatomic acoustic metamaterial with negative stiffness mechanism. *Engineering Structures* 271: 114939.
- Mančić A, Leykam D and Maluckov A (2023) Band relaxation triggered by modulational instability in topological photonic lattices. *Physica Scripta* 98(5): 055513.
- Murer M, Guruva SK, Formica G, et al. (2023) A multi-bandgap metamaterial with multi-frequency resonators. *Journal of Composite Materials* 57(4): 783–804.
- Newton PK and Keller JB (1987) Stability of periodic plane waves. *SIAM Journal on Applied Mathematics* 47(5): 959–964.
- Shu Y and Lien I (2006) Analysis of power output for piezoelectric energy harvesting systems. *Smart Materials and Structures* 15(6): 1499.
- Wu Z and Wang KW (2019) On the wave propagation analysis and supratransmission prediction of a metastable modular metastructure for non-reciprocal energy transmission. *Journal of Sound and Vibration* 458: 389–406.